Proceedings of the 1st Global Power and Propulsion Forum
GPPF 2017
Jan 16-18, 2014, Zurich, Switzerland
www.pps.global

GPPF-2017-51

A COMBINED EXPERIMENTAL AND NUMERICAL ANALYSIS OF THE WAKE STRUCTURE AND PERFORMANCE OF A H-SHAPED DARRIEUS WIND TURBINE

Alessandro Bianchini
Dept. of Industrial Engineering
Università degli Studi di Firenze
bianchini@vega.de.unifi.it
Firenze, Italy

Francesco Balduzzi
Dept. of Industrial Engineering
Università degli Studi di Firenze
balduzzi@vega.de.unifi.it
Firenze, Italy

Giovanni Ferrara
Dept. of Industrial Engineering
Università degli Studi di Firenze
giovanni.ferrara@unifi.it
Firenze, Italy

Lorenzo Ferrari
DESTEC
Università degli Studi di Pisa
lorenzo.ferrari@unipi.it
Pisa, Italy

Giacomo Persico
Dipartimento di Energia
Politecnico di Milano
giacomo.persico@polimi.it
Milano, Italy

Vincenzo Dossena
Dipartimento di Energia
Politecnico di Milano
vincenzo.dossena@polimi.it
Milano, Italy

Lorenzo Battisti
Dept. of Civil, Environ. and Mech. Engineering
Università di Trento
lorenzo.battisti@unitn.it
Trento, Italy

ABSTRACT

The Darrieus concept is increasingly welcome by both researchers and manufacturers of wind turbines, especially in view of small-size installations in the built environment or large-scale offshore rotors mounted on floating platforms. To achieve a more efficient, structurally sound and cost-effective design of Darrieus Vertical Axis Wind Turbines, numerical techniques making use of Computational Fluid Dynamics are considered as the most promising tool, since they provide a detailed and comprehensive representation of the flow, which is instrumental for the understanding of the unsteady aerodynamics of the rotor.

In this study, a two-dimensional U-RANS computational model was applied to analyze both the overall performance and, especially, the wake characteristics on the mid plane of a H-shaped Darrieus VAWT for microgeneration. The turbine was studied experimentally in a large-scale, open-jet wind tunnel, including both performance and wake measurements, in the frame of a comprehensive activity oriented to the construction of an experimental benchmark for VAWT simulations. Thanks to the availability of such a unique set of experimental data, systematic comparisons between simulations and experiments were carried out, highlighting the main aerodynamic phenomena and flow macro-structures and discussing the prediction capabilities of the numerical model.

On these bases, the present study is considered of interest for the scientific community working in this field, especially as a first support to future analyses aimed at improving the understanding of the unsteady aerodynamics taking place past Darrieus wind turbine blades.

INTRODUCTION

Vertical Axis Wind Turbines (VAWTs), especially in the Darrieus configuration, have been recently identified as suitable for new types of applications such as small-scale installations in complex terrains (e.g. the urban environment, see Balduzzi et al [1]) or offshore large floating platforms (e.g. Borg et al [2]). The reasons for this increasing success are mainly connected to the superior mechanical simplicity, ease of installation and maintenance, afforded by the positioning of generation equipment at ground level (Paraschivoiu [3]). Moreover, Darrieus VAWTs present good handling of turbulent and complex flows, with low noise emissions and high reliability (A. Bhutta et al [4]). Unfortunately, the efficiency of Darrieus turbines still lacks from that of conventional horizontal axis wind turbines. To improve efficiencies further, a more in depth understanding of the physical phenomena that govern Darrieus turbine behavior is needed. Some of these phenomena, e.g. dynamic stall (Simao-Ferreira et al [5]) or flow curvature effects (Rainbird et al [6]), are indeed not completely understood and so limited corrections, or no correction at all, are applied for them when designing the rotors.

Within this context, thanks to the increasing computational resources, CFD can play a fundamental role in enhancing the comprehension of the fluid structures past these rotating blades, since it represents the only model able to provide a detailed and comprehensive representation of the flow. Due to the complexity of this type of simulations, however, the possibility of having reliable and detailed experimental data to be used as validation test cases is pivotal to tune the numerical tools. Within this framework,

an extended experimental research program on VAWTs was carried out in collaboration with the University of Trento, in the frame of a National founded project, whose results are partially documented in Dossena et al [7] and Persico et a. [8]. Throughout this project, two rotor architectures (closed-troposkien-blade and open-H-blade) were tested in several flow conditions, with the aim to give insights into the different aerodynamics of the two configurations and to make results available as an experimental benchmark for future projects on similar machines. In the present study, thanks to the availability of such a unique set of experimental data, a systematic cross-comparison was carried out between the experimental results of the H-shaped rotor at the mid plane and the numerical ones coming from a two-dimensional U-RANS computational model developed by some of the authors in the last few years (e.g. Balduzzi et al [9]). The main aerodynamic phenomena are highlighted and the prediction capability of the numerical model is discussed.

One may notice that the use of two-dimensional U-RANS simulations is probably not the most appropriate approach to this kind of analyses since 2D simulations are deemed to produce vortices that are more coherent and less prone to breakdowns than real 3D ones. The present research on Darrieus VAWTs is indeed trying to move the CFD simulations towards fully three-dimensional analyses, which are however still hampered by the enormous calculation resources needed. On the other hand, recent studies (e.g. [6]) showed that the approach here proposed can give an accurate estimation of the aerodynamics of these machines, even in terms of instantaneous torque profile. On these bases, it is here thought to be also exploitable to assess the main flow structures attended in the wake of a H-Darrieus rotor.

VAWT TEST MODEL

The turbine prototype considered in this study is a three-blade, H-shaped Darrieus VAWT. The blades are connected to the support steel pole by two aluminium spokes, as shown in Fig. 1.

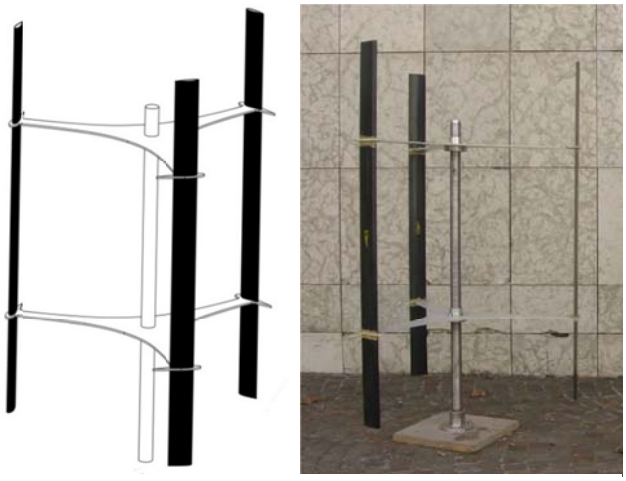

(a) **(b)**

Figure 1. Design (a) and picture (b) of the H-shaped VAWT under consideration.

The rotor has a swept area of 1.5 m^2 (H x D, 1.5 m x 1.028 m), and it is equipped with dihedral blades composed by un-staggered NACA0021 profiles (c = 0.086 m). Full details on the laboratory model are reported in [7].

EXPERIMENTAL CAMPAIGN

In this paper, CFD simulations are thoroughly compared against wind tunnel measurements performed some of the authors in a previous, but recent, experimental campaign. In the frame of this experimental activity, aerodynamic as well as performance measurements were carried out to investigate the turbine wake and performance. A brief review of the experimental layout is reported in the following section, while full details on the test campaign can be found in [7].

Wind Tunnel

The measurements reported in this paper were performed in the large-scale wind tunnel of the Politecnico di Milano (Italy). It consists of a closed-loop facility, whose test section (4.00 m wide, 3.84 m high and 6.00m long) allows the aerodynamic characterization of real-scale wind turbines for micro-generation, up to a maximum wind speed of 55 m/s. A combination of honeycombs and anti-turbulence screens provides high flow quality, resulting in a freestream turbulence intensity at the inlet lower than 1%.

Since the solid blockage of the rotor amounts to 10% of the wind tunnel chamber, a relevant blockage effect was observed in conventional wind tunnel tests performed in confined (or “closed chamber”) configuration. To limit the blockage, further tests were carried out using a "free jet" (or “open chamber”) configuration, by removing the test room upstream of the diffuser leading to the fans, and installing the rotor directly facing the upstream tunnel. Application of classical correlations for free-jet blockage suggests that the blockage is negligible in the present case (below a few %) [7]; therefore, free-jet wind tunnel results are believed to be representative of the open field configuration, and are here considered for comparison with CFD simulations.

Instrumentation and Data Processing

The experimental turbine performance was obtained by combining an absolute encoder for rotational speed measurements and a precision torque meter, mounted between elastic joints, to measure the torque transmitted through the shaft.

Data were registered using a Compact-RIO (National Instruments) data acquisition board, setting a sampling frequency of 2 kHz. Recorded time series lasted 3 minutes for each working condition, in order to guarantee a sufficient amount of data for time-averaging. Measurement uncertainty was computed by resorting to the classical error propagation theory; the reader is referred to [7] for the quantification of the uncertainty as a function of the TSR. To investigate the velocity magnitude and the turbulence field in the wake, two single-sensor hot wire probes were traversed downstream of the rotors. Uncertainty in the velocity measurements resulted about 2% after calibration in a low-speed jet. The first hot wire probe was mounted aligned with the wind speed

direction, thus exposing the wire normal to the wind to measure directly the velocity magnitude. The second probe was mounted in the vertical direction and was rotated during operation around its own axis to measure the transversal velocity components, by exploiting the angular sensitivity of wire. The so-called "triple decomposition" was performed on hot wire data, by extracting the time-averaged, phase-resolved, and turbulent components of the velocity, as discussed by Persico et al [8]. The phase-resolved component was obtained by ensemble averaging the velocity signals, using the encoder as a key-phasor. The streamwise turbulence intensity was determined by extracting the unresolved unsteady fluctuations of the velocity signal. A pneumatic five-hole probe was also applied throughout the tests to measure the pressure level and the 3D flow direction. Measured pressure values confirmed the absence of blockage-induced over-speeds outside the wake region; flow angle measurements with the vertical hot wire and the pneumatic probe also indicated negligible transversal and vertical velocity components in the wake at midspan.

NUMERICAL SIMULATIONS

The two-dimensional simulations presented in this paper were carried out using the commercial code ANSYS® FLUENT® [10]. The time-dependent unsteady Reynolds-averaged Navier–Stokes (U-RANS) approach was adopted in a pressure-based formulation. The fluid was air, which was modeled as an ideal compressible fluid following the suggestion of Balduzzi et al [9]. Inlet air conditions were the same monitored during the experimental tests, i.e. a pressure of 1.01×10^5 Pa, a temperature of 293 K and an inlet turbulence level of 1%. Some of the authors have recently presented (Balduzzi et al [9]) the assessment and validation of the main settings for a proper CFD simulation of Darrieus wind turbines using the FLUENT® code, whose accuracy has been also successfully verified by means of experimental data (Balduzzi et al [11]). Moreover, in recent works (Balduzzi et al [12] and Bianchini et al [13]) the accuracy of the proposed numerical approach has been verified exactly on the same case study considered here. For the sake of completeness, the main numerical settings are briefly summarized below. The turbulence closure was achieved by means of the k-ω shear stress transport (SST) model (Menter [14]), coupled with the Enhanced Wall Treatment embedded in the FLUENT® code for the computation of the boundary layer in the near-wall regions; since the y^+ was constantly kept < 1 in the boundary layer, the linear law of the wall is actually used.

The Coupled algorithm was employed to handle the pressure-velocity coupling. The second order upwind scheme was used for the spatial discretization of the whole set of RANS and turbulence equations, as well as the bounded second order for time differencing to obtain a good resolution (Amet et al [15]). The global convergence of each simulation was monitored by considering the difference between the mean values of the torque coefficient over two subsequent revolutions: according to Balduzzi et al [11], the periodicity error threshold was set to 0.1%.

To simulate the rotation of the turbine, the sliding mesh technique was employed, i.e. the computed domain was split into a circular zone containing the turbine, rotating with the same angular velocity of the rotor, and an outer rectangular fixed zone, determining the overall domain extent. The final dimensions of both domains were defined, according to the sensitivity analysis reported by Balduzzi et al [9], so to allow a full and unconstrained development of the turbine wake. In this way, CFD results can be properly compared to experiments obtained in unconfined configuration. A velocity-inlet boundary condition was imposed at the inlet section (40D upwind from the revolution axis). The ambient pressure condition was imposed at the outlet boundary (100D downwind), while a symmetry condition was defined on lateral boundaries (30D).

In the present study, the finest mesh defined during the sensitivity analyses reported by Balduzzi et al [12] was used for all the three considered tip-speed ratios. Even if redundant at TSR=3.3, this refinement level indeed ensured a very accurate discretization of the whole area around the rotor, greatly limiting any bias error due to the numerical discretization. The mesh is of unstructured and hybrid type, with triangular elements in the core flow region, and an O-grid made of quads in the boundary layer. As discussed, the first element height was chosen to guarantee that the dimensionless wall distance at the grid nodes of the first layer above the blade wall does not exceed $y^+ \sim 1$. The expansion ratio for the growth of elements starting from the surface was kept below 1.1 to achieve good mesh quality. The airfoil surface was discretized with 1400 nodes, resulting in 1.2×10^6 elements for the rotating region, while the stationary region was discretized with 2.0×10^5 elements. The mesh characteristics fully accomplish the criteria based on dimensionless thresholds proposed by Balduzzi et al [16]. Based on the same criteria, in order to limit the Courant Number in proximity of the blades, an angular timestep of 0.21° was used, i.e. the finest one identified by Bianchini et al in [13]. With the described settings, the calculation time to achieve a complete revolution of the rotor is around 24 hours in a 16 CPUs (2.8 MHz each) calculation center. The required number of revolutions to achieve a periodic solution is dependent on the TSR, varying from 10 to 20 revolutions.

Figure 2 finally shows some visual details of the mesh in the rotating region (a) and near the leading edge (b).

RESULTS AND DISCUSSION

To assess the prediction capability of the CFD approach, Fig. 3 compares the curve of experimental power coefficient c_P, defined according to Eq. 1 and measured by Dossena et al [7], with the one obtained with present simulations.

$$c_P = \frac{P}{\frac{1}{2}\rho A V_0^3}. \quad (1)$$

It is worth remarking that numerical results were corrected to account for the parasitic torque of the supporting struts of the rotor, which were of course not simulated in the two-dimensional approach.

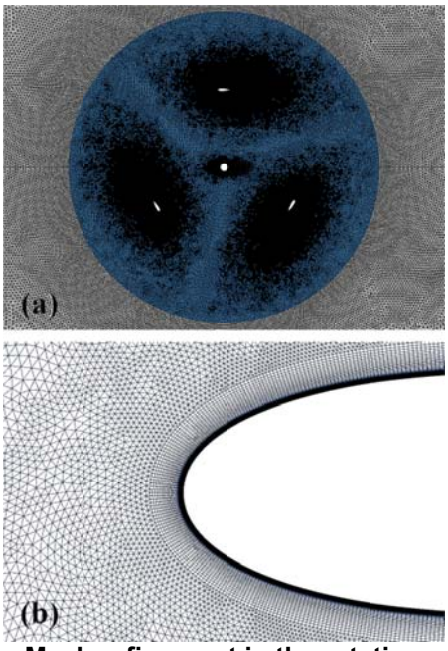

Figure 2 - Mesh refinement in the rotating region (a) and near the leading edge (b).

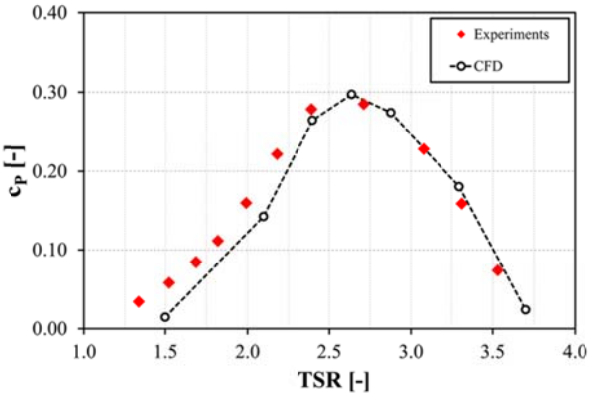

Figure 3 - Comparison between experiments from [7] and present CFD simulations corrected for the struts' parasitic torque.

The correction was introduced by resorting to the original one-dimensional model developed by Bianchini et al [17], assuming a rectangular shape of the struts section. As a matter of fact, the model considers a constant equivalent drag coefficient for the section and assumes that the induced aerodynamic drag during the revolution is given by the projection of the relative speed (variable with the radius and calculated with a multitubes BEM approach for each azimuthal position) on the tangential direction. For further detail on the model, the reader is referred to the analyses of the same authors in [17] and [18], where the reliability of the model was assessed by means of experimental tests in the wind tunnel.

Upon examination of the figure, sound agreement between experiments and simulations is apparent. In particular, numerical results are able to reproduce properly the power curve over the entire range of TSRs of interest, both in terms of qualitative trend and c_P values. A little discrepancy, quite common in all CFD simulations of Darrieus VAWTs, can be noted at low tip-speed ratios; in this region of the curve, the airfoils work in stalled conditions for a considerable fraction of the revolution, with severe flow separation phenomena and large-scale vortices detaching even from the leading edges of the airfoils. In these conditions, additional elements like the surface roughness, the trailing-edge refinement in the experimental model, etc. can play a fundamental role in setting the characteristics of such separations, which are however pivotal for the final torque production. Overall, by virtue of these results, the CFD approach can be considered reliable for the purposes of the present study.

To analyse the wake characteristics, three relevant TSRs were selected for analysis, for which detailed flow measurements were available. Based on the indications of [7], the tip-speed ratios of 1.5, 2.4 and 3.3 were considered for comparison, corresponding to a wind speed V_0 of 14.2 m/s, 9.0 m/s and 6.5 m/s, respectively, having assigned a constant angular speed of the turbine equal to 400 rpm.

Figure 4 compares the CFD-based torque coefficient profiles, c_T (Eq. 2), for the three investigated conditions.

$$c_T = \frac{T}{\rho A \frac{D}{4} V_0^2} . \quad (2)$$

By looking at the torque profiles, one can readily notice that the TSR=1.5 condition represents a highly unstable operating point, with an abrupt stall onset in the upwind zone (around approximately ϑ=60°), followed by intense ripples due to the onset and the subsequent propagation of macro-vortices detaching from the blades (see Rainbird et al [6]). In particular, as will be discussed later on in the study, the deep stall in the second quadrant originates strong macro-vortices that are convected downstream by the flow and interact with the downstream blades, resulting in the intense ripples shown in the torque profile.

The TSR=2.4 condition still lies in the unstable part of the operating curve, but the upwind peak is now shifted towards ϑ=90°, i.e. where it is commonly located for this kind of airfoil during conventional turbine operation. After stall occurs, the trend is again quite steep, with a negative torque region between ϑ=120° and ϑ=180° and large ripples downwind.

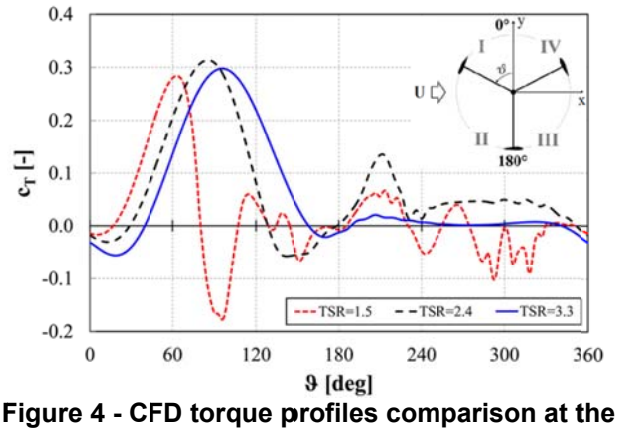

Figure 4 - CFD torque profiles comparison at the three investigated TSRs.

Finally, TSR=3.3 represents a stable functioning condition, with no evidence of abrupt stall, even if the torque extraction is strongly unbalanced towards the upwind zone, as typically found for three-blade rotors of similar solidity.

To understand the physics underlying these trends, the possibility of having experimental measurements of the flow field becomes crucial In particular, for all the three functioning points comparisons were made between the numerical results and the experiments in terms of dimensionless velocity (V/V_0) and turbulence intensity (I_{TU}). CFD data have been acquired in correspondence of virtual rakes positioned exactly at the same distance from the shaft of the experimental traverses, i.e. "near" 0.75D downstream and "far" 1.5D downstream the shaft. At each section, 100 equally spaced points were acquired at a frequency of 10 kHz for at least 3 revolutions. Based on these data, averaged profiles were also calculated and added to the comparisons.

Figure 5 reports the results at TSR=1.5 for the near traverse, in the form of measured and computed velocity and turbulence profiles. Super-imposed to the computed averaged profiles, the unsteady dispersion is also reported. Good agreement is generally found between simulations and experiments, in terms of wake width and deficit as well as in terms of flow and turbulence morphology inside the wake. From an in-depth analysis of the trends, it is worth remarking that CFD data present a high dispersion, especially in three positions, i.e. around Y/D=-0.4, Y/D=-0.2 and 0.1 <Y/D<0.4. In these positions, both the velocity and the turbulence fields present wide ripples, whose nature can be comprehended by looking at the computed velocity field, whose distribution is reported in Fig. 6 for a given instant.

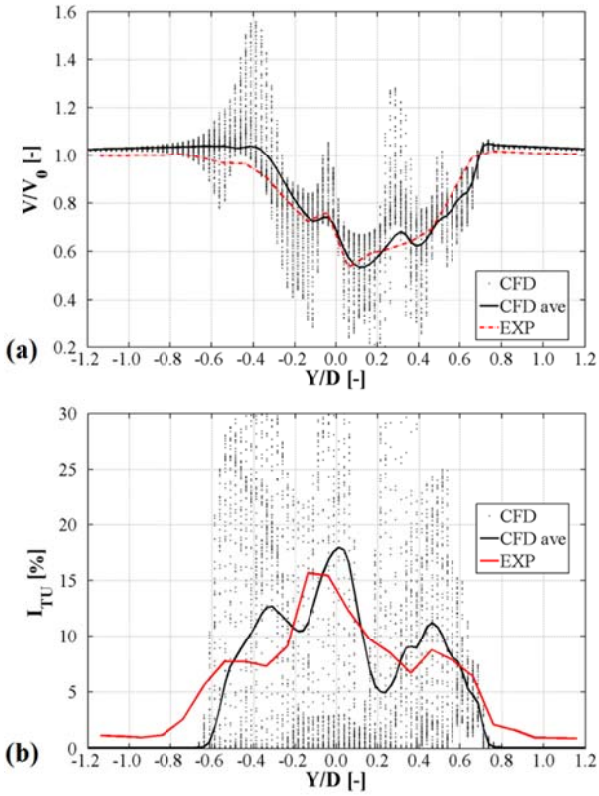

Figure 5 - Near traverse: dimensionless velocity (a) and turbulence intensity (b) at TSR=1.5.

Upon examination of the figure, one can notice that the first two ripples correspond to the onset and the propagation of strong macro vortices connected to the deep stall experienced by the airfoils, already discussed in Fig. 4.

The third ripple (located approximately behind the tower) is instead connected to another set of vortices that originate from the airfoil trailing edge as soon as the incidence angle is decreasing again towards values which allow the flow to reattach to the blades. Both these two phenomena have a major impact on the overall performance of the rotor. Fully comparable trends were also found for the far traverse (Fig. 7), with the main flow structures still noticeable, even though with a general reduction of the fluctuations intensity.

Considering the condition corresponding to TSR=2.4, Fig. 8 reports the results again for the near traverse.

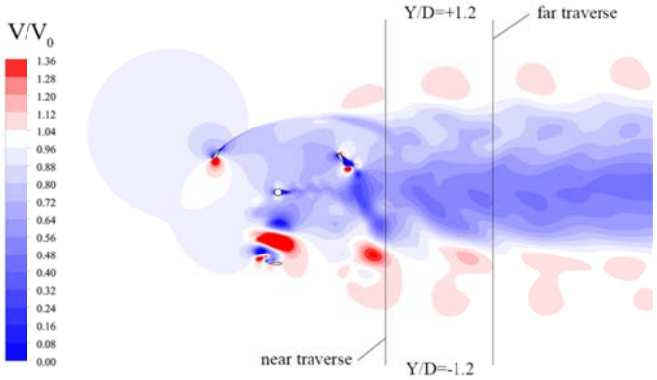

Figure 6 - Instantaneous velocity field at TSR=1.5.

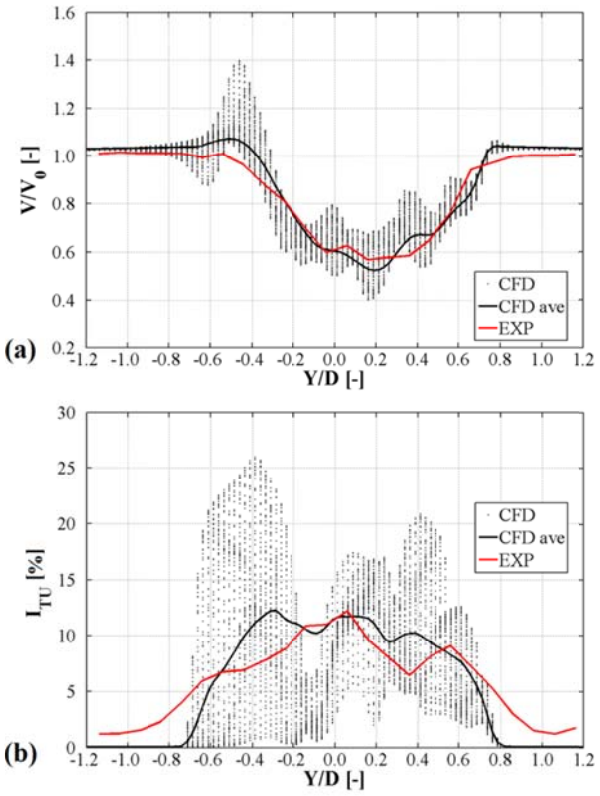

Figure 7 - Far traverse: dimensionless velocity (a) and turbulence intensity (b) at TSR=1.5.

In this case, the velocity profile is smoother and the data dispersion is lower. In further detail, as testified by the snapshot of the instantaneous velocity field reported in Fig. 9, a more uniform wake structure was predicted by CFD. Even if the overall accuracy of simulations is still good in terms of wake width, a discrepancy can be here noticed in the region behind the rotor, where experiments revealed a velocity deficit higher than that predicted numerically. Such deviation might be connected to a higher impact of the interaction between the flow and the tower. This evidence is in agreement with the slightly lower value of the predicted power coefficient previously discussed in Fig. 3.

A general decrease of the turbulence level can be also noticed in Fig.8(b). With respect to the lower TSR, the turbulence intensity profile predicted by CFD is almost flat and of low magnitude in the center of the wake, with two, clearly marked, peaks at the two sides of the wake itself; the position and relative intensity of these peaks is again in remarkable agreement with experiments. In tunnel measurements, a further peak is however distinguishable at the center of the wake, again suggesting a stronger influence of the tower.

To better understand the nature of the two lateral peaks, Fig. 10 reports the instantaneous distribution of turbulence intensity in the same instant in time of Fig. 9.

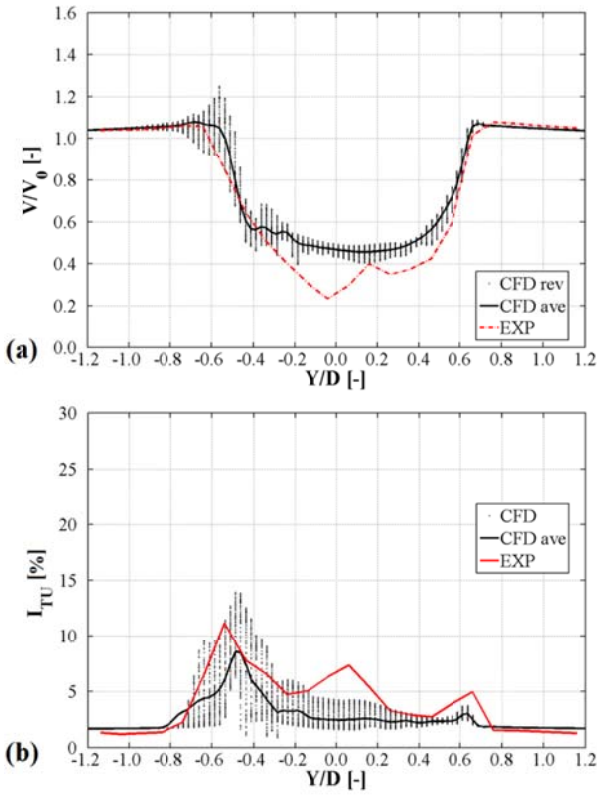

Figure 8 - Near traverse: dimensionless velocity (a) and turbulence intensity (b) at TSR=2.4.

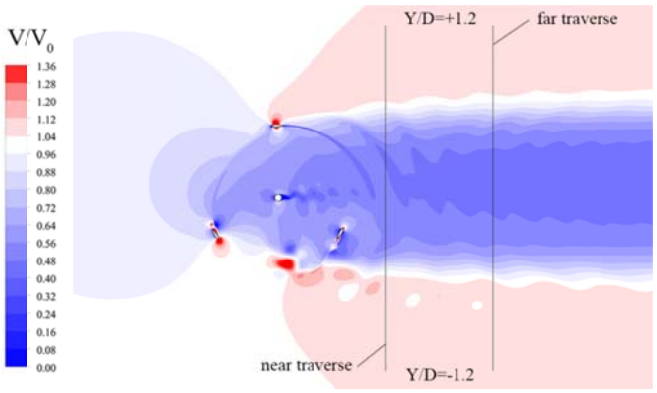

Figure 9 - Instantaneous velocity field at TSR=2.4.

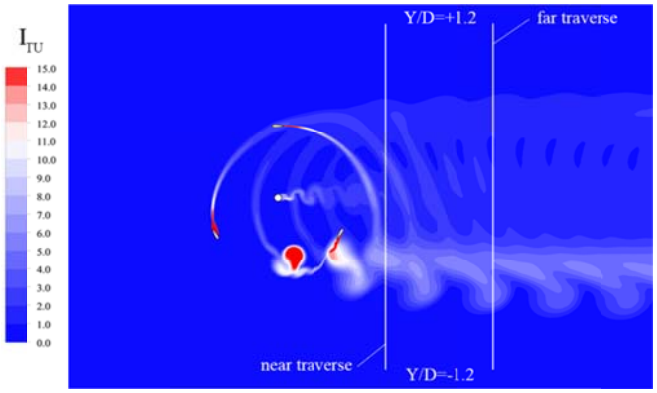

Figure 10 - Instantaneous turbulence intensity field at TSR=2.4.

Figure 10 clearly suggests that the two local increases of turbulence intensity are related to the propagation of the two different vortices, already noticed at TSR=1.5, that are now even more evident thanks to the vorticity analysis. The more intense one, located approximately at *Y/D*=-0.5, is indeed more precisely related to the macro vortices generated by the deep stall conditions experienced by the airfoil in the last region of the upwind part of the revolution; once they are detached from the airfoil surface, the vortices are then convected downstream by the main flow, with the same mechanism discussed in Fig. 6. The other peak is instead related to the flow reattachment in the last part of the downwind region as soon as the incidence angle decreases below the stall one.

The main phenomena described for the near traverse are again clearly distinguishable also in the far one (Fig. 11), with an even more pronounced discrepancy for the velocity deficit in the wake in correspondence to the central tower.

Finally, Fig. 12 and Figure 13 report the results for the at TSR=3.3 for the near and far traverse, respectively.

As discussed, in this high-loaded TSR conditions the airfoils do not exhibit the onset of deep stall and the flow tends to remain attached to the airfoil walls during the whole revolution, with no formation of vortical structures similar to those described for lower TSRs. The data dispersion and the turbulence levels are accordingly lower.

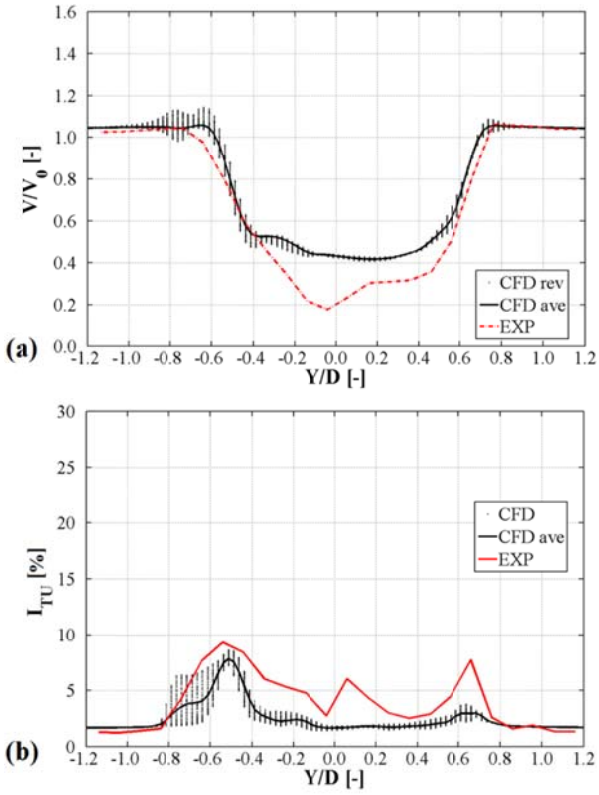

Figure 11 - Far traverse: dimensionless velocity (a) and turbulence intensity (b) at TSR=2.4.

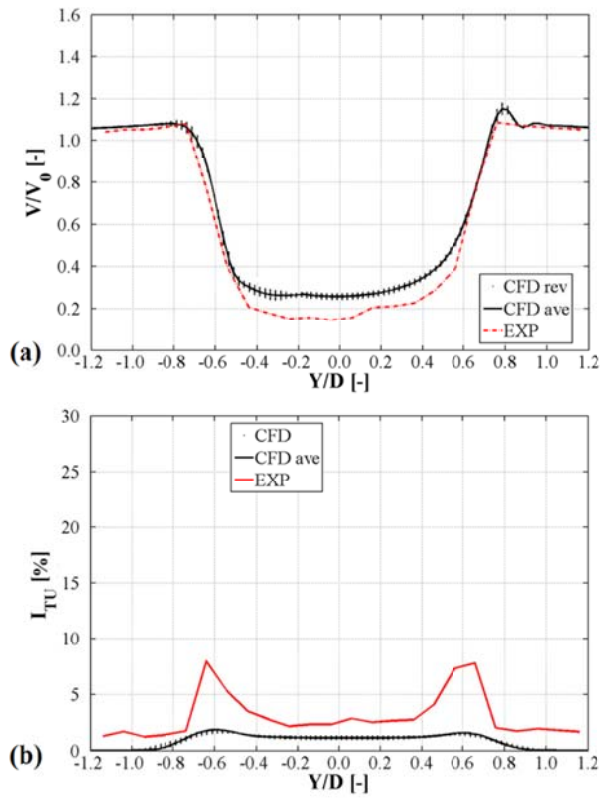

Figure 12 - Near traverse: dimensionless velocity (a) and turbulence intensity (b) at TSR=3.3.

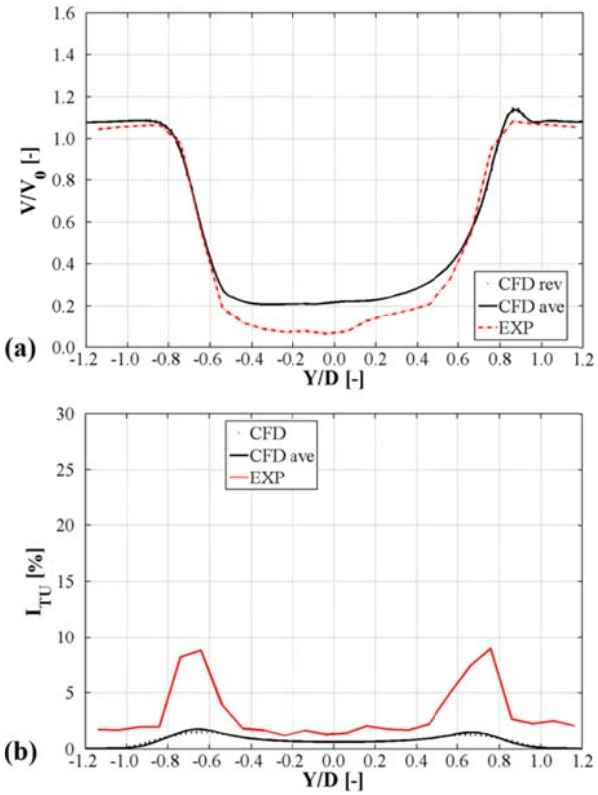

Figure 13 - Far traverse: dimensionless velocity (a) and turbulence intensity (b) at TSR=3.3.

Experiments again showed a slightly more intense velocity deficit in the wake, even if the overall comparison between data is satisfying. As mentioned for the two previous TSR conditions, the velocity profiles remain substantially coherent with those measured at the near traverse, with even smoother trends and lower dispersion.

CONCLUSIONS

In the present study, a comprehensive set of flow measurements inside the wake of a Darrieus vertical-axis wind turbine have been compared with two-dimensional CFD simulations of the same rotor in the mid plane.

Overall, an interesting agreement was found between measurements and simulations, even if a 2D U-RANS approach is usually thought to be not fully suitable for these analyses. In particular, the CFD data were able to correctly predict the performance of the turbine and also to highlight some main flow structures whose effects were fully compatible with experimental trends.

In particular, it has been shown that at low TSRs the wake is characterized by very intense ripples, due to the passage of macro vortices detaching from the blades either in the upwind region after the stall angle is reached, or in the downwind region as soon as the flow tends to re-attach to the blade. For an intermediate TSR, intense turbulence and some ripples are still clearly distinguishable in reason of the wide range of incidence angles experienced by the airfoils, which may lead to stall onset. Finally, for high TSRs, typical of the stable part of the functioning curve, the wake is more regular and smoother with less intense ripples and turbulence, even if

the velocity deficit is now increased due to the higher load experienced by the turbine.

NOMENCLATURE

A	turbine swept area	[m^2]
c_P	power coefficient	[-]
c_T	torque coefficient	[-]
CFD	Computational Fluid Dynamics	
D, R	turbine diameter, radius	[m]
I_{TU}	turbulence intensity	[m]
k	turbulent kinetic energy	[m^2s^{-2}]
P	power	[W]
RANS	Reynolds-Averaged Navier-Stokes	
SST	Shear Stress Transport	
T	torque	[Nm]
TSR	Tip-Speed Ratio	
V	wind speed	[m/s]
VAWT	Vertical Axis Wind Turbines	
y^+	dimensionless wall distance	[-]

Greek letters

ϑ	azimuthal angle	[deg]
ρ	air density	[kg/m^3]
ω	Specific turbulence dissipation rate	[s^{-1}]
Ω	revolution speed	[rpm]

Subscripts

0	value at inlet

ACKNOWLEDGMENTS

Thanks are due to Prof. Ennio Antonio Carnevale of the University of Florence for supporting this study, and to Dr. Andrea Tanganelli for his support in the CFD simulations.

The authors would like also to acknowledge the Company Tozzi-Nord Wind Turbines for the rotor model and the technicians and collaborators of Universitá di Trento and Politecnico di Milano for their precious support before and during the tests.

REFERENCES

[1] Balduzzi, F, Bianchini, A, Carnevale, EA, Ferrari, L and Magnani, S, "Feasibility analysis of a Darrieus vertical-axis wind turbine installation in the rooftop of a building," Applied Energy, 97, 2012, pp. 921–929

[2] Borg, M, Shires, A, and Collu, M, "Offshore floating vertical axis wind turbines, dynamics modelling state of the art. Part I: Aerodynamics", Renewable and Sustainable Energy Reviews, 39, 2014, pp. 1214-1225

[3] Paraschivoiu, I, Wind turbine design with emphasis on Darrieus concept, Polytechnic International Press, Montreal, Canada, 2002.

[4] Aslam Bhutta, MM, Hayat, N, Farooq, AU, Ali, Z, Jamil, ShR, and Hussain, Z, "Vertical axis wind turbine – A review of various configurations and design techniques," Renewable and Sustainable Energy Reviews, 16(4), 2012,1926-1939

[5] Simao-Ferreira, C, van Zuijlen, A, Bijl, H, van Bussel, G, and van Kuik, G, "Simulating dynamic stall on a two-dimensional vertical-axis wind turbine: verification and validation with particle image velocimetry data", Wind Energy, 13, 2010, pp. 1-17

[6] Rainbird. J, Bianchini, A, Balduzzi, F, Peiro, J, Graham, JMR, Ferrara, G, and Ferrari, L, "On the Influence of Virtual Camber Effect on Airfoil Polars for Use in Simulations of Darrieus Wind Turbines," Energy Conversion and Management, 106(December 2015), 2015, pp. 373-384

[7] Dossena, V, Persico, G, Paradiso, B, Battisti, L, Dell'Anna, S, Brighenti, A and Benini, E, "An Experimental Study of the Aerodynamics and Performance of a Vertical Axis Wind Turbine in a Confined and Unconfined Environment", 2015, ASME Journal of Energy Resources Technology, 137(5) 2015, paper code 051207 (12 pages)

[8] Persico, G, Dossena, V, Paradiso, B, Battisti, L, Brighenti, A and Benini, E, "Three-Dimensional Character of VAWT Wakes: an Experimental Investigation for H-Shaped and Troposkien Architectures", Proc. of the ASME Turbo Expo 2016, Seoul, South Korea, June 13-17, 2016.

[9] Balduzzi, F, Bianchini, A, Maleci, R, Ferrara, G and Ferrari, L, "Critical issues in the CFD simulation of Darrieus wind turbines", Renewable Energy, 85(01), 2016, pp. 419-435

[10] ANSYS®, Inc., 2015, "FLUENT® Theory Guide", release 16.0

[11] Balduzzi, F, Bianchini, A, Maleci, R, Ferrara, G, and Ferrari, L, "Blade Design Criteria to Compensate the Flow Curvature Effects in H-Darrieus Wind Turbines", J. of Turbomachinery, 137(1), 201, pp. 011006-011006-10

[12] Balduzzi, F, Bianchini, A, Gigante, FA, Ferrara, G, Campobasso, MS, and Ferrari, L, "Parametric and Comparative Assessment of Navier-Stokes CFD Methodologies for Darrieus Wind Turbine Performance Analysis", Proc. of the ASME Turbo Expo 2015, Montreal, Canada, June 15-19, 2015

[13] Bianchini, A, Balduzzi, F, Ferrara, G, and Ferrari, L, "Aerodynamics of Darrieus wind turbines airfoils: the impact of pitching moment", J. of Engineering for Gas Turbines and Power, 2016, paper in press

[14] Menter, F, "Two-equation Turbulence-models for Engineering Applications," AIAA Journal, 32(8), 1994, pp. 1598–1605

[15] Amet, E, Maître, T, Pellone, C, and Achard, JL, "2D numerical simulations of blade-vortex interaction in a Darrieus turbine", J. of Fluids Engineering, 131(11), 2009, pp. 1-15

[16] Balduzzi, F, Bianchini, A, Ferrara, G, and Ferrari, L, "Dimensionless numbers for the assessment of mesh and timestep requirements in CFD simulations of Darrieus wind turbines," Energy, 97(15 February 2016), 2016, pp. 246-261

[17] Bianchini, A, Ferrari, L and Magnani, S, "Start-up behavior of a three-bladed H-Darrieus VAWT: experimental and numerical analysis", Proc. of the ASME Turbo Expo 2011, Vancouver, Canada, June 6-10, 2011.

[18] Bianchini, A, Balduzzi, F, Ferrara, G and Ferrari, L, "Influence of the blade-spoke connection point on the aerodynamic performance of Darrieus wind turbines", Proc. of the Turbo Expo 2016, Seoul, South Korea, June 13-17, 2016.